Experimental Proposal on Non-Hermitian Skin Effect by Two-dimensional Quantum Walk with a Single Trapped Ion

Waner Hou(侯琬儿)[1], Hao Tang(唐皓)[1], Qin Xu(许勤)[1], and Yiheng Lin(林毅恒)[1,2*]

[1]*CAS Key Laboratory of Microscale Magnetic Resonance and School of Physical Sciences, University of Science and Technology of China, Hefei 230026, China*
[2]*Hefei National Laboratory, University of Science and Technology of China, Hefei 230088, China*

(Received 25 January 2024; accepted manuscript online 15 March 2024)

Non-Hermitian Hamiltonians are widely used in describing open systems with gain and loss, among which a key phenomenon is the non-Hermitian skin effect. Here we report an experimental scheme to realize a two-dimensional (2D) discrete-time quantum walk with non-Hermitian skin effect in a single trapped ion. It is shown that the coin and 2D walker states can be labeled in the spin of the ion and the coherent-state lattice of the ion motion, respectively. We numerically observe a directional bulk flow, whose orientations are controlled by dissipative parameters, showing the emergence of the non-Hermitian skin effect. We then discuss an experimental implementation of our scheme in a laser-controlled trapped Ca^+ ion. Our experimental proposal may be applicable to research of dissipative quantum walk systems and may be able to generalize to other platforms, such as superconducting circuits and atoms in cavity.

DOI: 10.1088/0256-307X/41/4/040301

Quantum walk is proposed as the quantum analogy of classical random walk.[1] Unlike its classical counterpart, the superposition and interference of different paths in quantum walks result in many fundamentally distinct properties, e.g., as reviewed in Refs. [2,3]. One notable property is their capability to reach quadratic speed-up compared to classical random walks when spreading spatially, which leads to broad application in devising quantum algorithms outperforming classical ones, including searching algorithms,[4–7] solving constraint satisfaction problems,[8] NAND tree problems,[9] and graph isomorphism problems.[10,11] Quantum walks are also widely used in quantum simulation[12–15] and quantum communication.[16–18] The discrete-time quantum walk (DTQW) is a quantum counterpart of the discrete-time classical random walk.[1] In DTQWs, the walker hops in a discrete lattice at discrete times, while the walking directions are determined by the coin state.

DTQWs have been experimentally demonstrated in many physical platforms, such as photonic systems[19,20] and superconducting qubits.[21] In the last few years, ion trap platforms have provided key contributions to many experiments with high operational fidelity in quantum information processes.[22] The local vibrational motions of trapped ions show particle-like characteristics and undergo interference, being well suited for the investigation of particle propagation represented by DTQWs. One-dimensional (1D) quantum walks utilizing a vibrational mode of trapped ions with phase space lattice and Fock state lattice were experimentally demonstrated,[23,24] among which a coherent quantum walk consisting of up to 23 steps has been reported. Recent proposals extend such an implementation to study the quench dynamics of spin-orbit coupled systems and topological physics.[25,26]

Recent theoretical and experimental works have extended quantum walks to higher- dimensions,[27] which is beneficial to investigations of special phenomena in non-Hermitian systems, such as the non-Hermitian skin effect (NHSE) in higher dimensions,[28–31] many-body Fock states with two dimensions,[32] and in the generation of GKP states.[33] In particular, directional matter transport has been experimentally demonstrated in a two-dimensional (2D) quantum walk of photons,[34] which underlies the emergence of NHSE and has potential applications in topological transport and device design. If one can extend such an implementation to the motion of trapped ions as an alternative platform, then several established techniques can be applied to facilitate the experimental study of non-Hermitian physics, such as high-fidelity phonon state initialization, control, and detection, as well as the detection of Wigner function to indicate the coherence during walking. Considering implementation in trapped ions for 2D NHSE, previous experimental implementations utilizing Fock states suffer from the fact that the coupling of adjacent Fock states is site-dependent, giving rise to unwanted non-linearity for the walking process.[35] In addition, the connectivity of the Fock state basis in a single motional mode limits the walking sites to 1D. On the other hand, for previous implementation of quantum walk in the 1D motional phase space, there is a great potential to extend it to 2D for novel applications because the phase space intrinsically contains both the real and imaginary components.

In this Letter, we propose an experimental scheme to realize a 2D DTQW in the momentum phase space of a single trapped ion. As an example, we generalize the scheme

*Corresponding author. Email: yiheng@ustc.edu.cn
© 2024 Chinese Physical Society and IOP Publishing Ltd

in a previous experiment with photons[34] to the trapped ion system to show a possible implementation. We consider walking on both real and imaginary directions on the discretized coherent state lattice in the motional Hilbert space, which enables a direct generalization to study the NHSE in 2D. The coin Hilbert space can be implemented in a two-level system, as a control of the walking direction. Furthermore, by introducing the non-unitary gain-loss operators to the coin Hilbert space $\mathcal{H}_c$, we are able to investigate the dynamic properties of NHSE under open boundary conditions. Specifically, a directional bulk flow can be predicted in phase space, which is one of the major features of NHSE.[36–38] By adjusting the gain-loss parameters, the direction, strength, and shape of the directional bulk flow can be manipulated. Finally, to test the experimental feasibility of this 2D DTQW scheme, we numerically simulate the laser-ion interaction model of a single trapped ion to compose the Hilbert space $\mathcal{H}_c \otimes \mathcal{H}_p$, in which the calculation parameters are set within the corresponding experimental range.

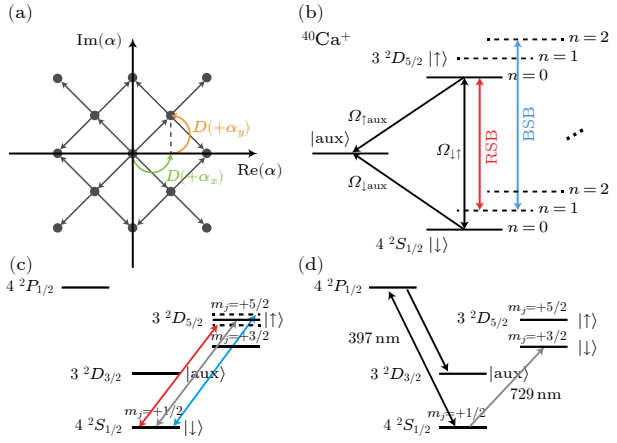

Fig. 1. Discrete-time 2D quantum walk on the momentum phase space of a single bounded $^{40}Ca^+$ ion. (a) The walker step space can consist of a series of coherent states $|\alpha\rangle$, with the spacing equal to unit movement $(\pm\alpha_x, \pm\alpha_y)$ along the real and imaginary axes. (b) An experimentally feasible scheme for 2D quantum walk on an ion trap. The walker's internal states $\{|\uparrow\rangle, |\downarrow\rangle\}$ are encoded in the metastable state $3d\ ^2D_{5/2}$ and ground state $4s\ ^2S_{1/2}$ of a $^{40}Ca^+$ ion, respectively. Phase space displacement can be controlled by the walker's internal states through laser-ion interaction under a bichromatic light field, which consists of blue-sideband transition and red-sideband transition. (c) The coin operator C and shift operators $S_{x,y}$ are constructed based on the transition between $D_{5/2,\,m_j=+5/2}$ and $S_{1/2,\,m_j=+1/2}$ of the $^{40}Ca^+$ ion. (d) $^{40}Ca^+$ ion-level scheme for the construction of gain-loss operators $M_{x,y}$. By temporarily mapping a portion of the $S_{1/2,\,m_j=+1/2}$ component to the $D_{5/2,\,m_j=+3/2}$ level, the components left in $S_{1/2}$ can be dissipated to the auxiliary state $D_{3/2}$ via $P_{1/2}$.

Discrete-Time 2D Quantum Walk. In discrete-time quantum walks, the walker state $|\psi\rangle$ is periodically driven by a Floquet operator $|\psi(N)\rangle = U^N|\psi(0)\rangle$, where U is the operator for each of the N discrete steps:

$$U = M_y S_y C M_x S_x C, \tag{1}$$

where the shift operators $S_{x,y}$ are defined as $S_j = |\downarrow\rangle\langle\downarrow| \otimes D(\alpha_j) + |\uparrow\rangle\langle\uparrow| \otimes D(-\alpha_j)$, and $D(\alpha_j) = e^{\alpha_j a^\dagger - \alpha_j^* a}$ labels the displacement operator of phase space in two additive directions $j\in\{x, y\}$ in the complex phase space, with $D^\dagger(\alpha_j) = D(-\alpha_j)$ and $D(\alpha_i)D(\alpha_j) = D(\alpha_i + \alpha_j)e^{i\Im\alpha_i\alpha_j^*}$. We denote $\{|n\rangle\}$ as the eigenstates of the harmonic oscillator. Starting from $|0\rangle$, repeated application of the shift operators with fixed $\pm\alpha_{j=x,y}$ gives rise to walking within a lattice of displaced coherent state $|\alpha_j\rangle = D(\alpha_j)|0\rangle = \sum_n e^{-|\alpha_j|^2/2}\frac{\alpha_j^n}{\sqrt{n!}}|n\rangle$, as shown in Fig. 1(a). The direction of displacements is decided by the walker's internal states with the basis of $\{|\uparrow\rangle, |\downarrow\rangle\}$, denoted as the coin states. These coin states are prepared under rotations from the coin operator $C = \frac{1}{\sqrt{2}}\begin{pmatrix}1 & 1\\ 1 & -1\end{pmatrix} \otimes I_n$, where $I_n = \sum_n |n\rangle\langle n|$. The gain-loss operators of the $j\in\{x, y\}$ directions are given by $M_j = \begin{pmatrix}e^{\gamma_j} & 0\\ 0 & e^{-\gamma_j}\end{pmatrix} \otimes I_n$, where γ_j introduces a direction dependence loss.

We analyze the directional displacement of the walker state by calculating the Wigner function of the oscillator state $|\psi\rangle$. The Wigner function is a phase-space quasiprobability distribution that plays an important role in characterizing oscillator states. It can be related to the expectation value of the parity operator with displacement β for the populations of the oscillator state $|\psi\rangle$, as $W(\beta) = \frac{2}{\pi}\sum_n(-1)^n\langle n|D^\dagger(\beta)\rho D(\beta)|n\rangle$ with $\rho = |\psi\rangle\langle\psi|$.[39] This relationship has been widely used in experiments to reconstruct the motional states of a trapped-ion oscillator.[40–42]

Experimental Scheme for a Trapped Ion. We consider a single trapped $^{40}Ca^+$ ion in a linear Paul trap. The motional degree of freedom is described by a Hamiltonian in the form of a quantum harmonic oscillator:

$$H_{\text{h.o.}} = \frac{\hat{p}^2}{2m} + \frac{1}{2}m\omega^2\hat{x}^2 = \hbar\omega\Big(a^\dagger a + \frac{1}{2}\Big), \tag{2}$$

where m is the mass of ion, ω is its angular oscillation frequency, and $a = \sqrt{\frac{m\omega}{2\hbar}}(\hat{x} + \frac{i}{m\omega}\hat{p})$ is the annihilation operator. The walker states are defined as the displaced coherent state $|\alpha\rangle$ in the motional dimension. The walker's coin states $\{|\uparrow\rangle, |\downarrow\rangle\}$ are encoded in the metastable state $3d\ ^2D_{5/2,\,m_j=+5/2}$ and ground state $4s\ ^2S_{1/2,\,m_j=+1/2}$ in the $^{40}Ca^+$ ion, respectively, as shown in Fig. 1(c). Thereby, we can encode an optical qubit in the coin Hilbert space $\mathcal{H}_c$ on the basis of Pauli matrices $\sigma_{x,y,z}$. A resonant laser beam interacting with the two-level ion implements the unitary operation:

$$R(\theta, \phi_l) = \begin{pmatrix}\cos\frac{\theta}{2} & -ie^{-i\phi_l}\sin\frac{\theta}{2}\\ -ie^{i\phi_l}\sin\frac{\theta}{2} & \cos\frac{\theta}{2}\end{pmatrix}, \tag{3}$$

which corresponds to a rotation of an angle θ around an axis at azimuthal angle ϕ_l in the equatorial plane on the Bloch sphere. Therefore, the coin operator C can be constructed using a resonant laser by first driving a σ_y-rotation of $\theta = \pi/2$, and then a σ_x-rotation of $\theta = \pi$, forming $C = -iR(\pi, \phi_l = 0)R(\pi/2, \phi_l = \pi/2)$.[43]

To introduce the non-unitary gain-loss operators $M_{x,y}$ to the coin Hilbert space $\mathcal{H}_c$, we can apply a dissipative process via an auxiliary state.[35] As shown in Fig. 1(b), by using two laser beams that effectively pump a portion of the population of the metastable state $D_{5/2}$ and

ground state $S_{1/2}$ to the auxiliary state $|\text{aux}\rangle$, respectively, we obtain the effective evolution operator on the internal states $M_j = e^{\gamma_j}|\uparrow\rangle\langle\uparrow| + e^{-\gamma_j}|\downarrow\rangle\langle\downarrow|$, up to a global dissipative identity. As an example, in Fig. 1(d) we consider the auxiliary state at the $D_{3/2}$ manifold. The pumping process can be achieved by first applying a shelving pulse with resonant 729 nm lasers, where a portion of the $S_{1/2,\,m_j=+1/2}$ component for the coin states is mapped temporarily to the other levels of the $D_{5/2}$ manifold, e.g., to the $D_{5/2,\,m_j=+3/2}$ level, while the components to be dissipated are mapped to the $S_{1/2}$ manifold. Then a pumping laser of 397 nm couples the $S_{1/2}$ to the excited $P_{1/2}$ states, which quickly decay to the $D_{3/2}$ manifold. Finally, resonant 729 nm lasers are applied to map the remaining populations in the $D_{5/2,\,m_j=+3/2}$ manifold back to the coin basis, finishing the dissipation process. The dissipation rate γ_j is related to the coupling strength $\Omega_{\uparrow\text{aux},\,\downarrow\text{aux}}$ and pumping time t between the walker's internal states $\{|\uparrow\rangle, |\downarrow\rangle\}$ with the auxiliary state $|\text{aux}\rangle$. For example, if a loss operator with $\gamma_x = +0.5$ needs to be introduced during the walking in the x direction, then after the controlled displacement S_x, only the laser that pumps the $|\downarrow\rangle$ state to the auxiliary state $|\text{aux}\rangle$ is turned on for a duration time $\cos(\Omega_{\downarrow\text{aux}}t/2) = e^{-2|\gamma_x|}$. Therefrom, while the population in the $|\uparrow\rangle$ state is unchanged, the population in the $|\downarrow\rangle$ state reduces to $c_\downarrow(t) = e^{-2|\gamma_x|}c_\downarrow(0)$, and one can find that after normalization an effective loss operator $M_x = e^{\gamma_x}|\uparrow\rangle\langle\uparrow| + e^{-\gamma_x}|\downarrow\rangle\langle\downarrow|$ is constructed. Similarly, if a gain operator with $\gamma_x = -0.5$ needs to be introduced, then the laser that pumps the $|\uparrow\rangle$ state to the auxiliary state $|\text{aux}\rangle$ should be turned on for a duration time $\cos(\Omega_{\uparrow\text{aux}}t/2) = e^{-2|\gamma_x|}$ to change the population in the $|\uparrow\rangle$ state to $c_\uparrow(t) = e^{-2|\gamma_x|}c_\uparrow(0)$.

Phase space displacement controlled by the walker's internal states can be achieved through laser-ion interaction Hamiltonian combining the two-level ion and the harmonic oscillator model.[44] In the ion's rest frame, an additional frequency modulation of the incoming laser light shift is introduced because of the ion's harmonic oscillation, which allows for a joint manipulation of the ion's internal spin states and external motional states. The laser-ion interaction Hamiltonian under the rotating wave approximation yields:

$$H_{\text{int}} = \hbar\frac{\Omega}{2}\{\sigma_+ e^{-i(\delta t+\phi_l)} \otimes \exp[i\eta(ae^{-i\omega t} + a^\dagger e^{i\omega t})] + \text{h.c.}\}, \quad (4)$$

where Ω is the Rabi frequency, δ is the laser detuning frequency, and $\eta = kx_0\cos\theta = k\sqrt{\frac{\hbar}{2m\omega}}\cos\theta$ is the Lamb-Dicke factor which accounts for the ratio of ion's motional ground state wave packet size x_0 and laser's wavelength $\lambda = 2\pi/k$, as well as the angle θ between ion's motional direction and laser direction. By introducing two superimposed laser fields at positive and negative detuning $\delta = \pm\omega$ from the resonant frequency with the same Rabi rate $\Omega_{\uparrow\downarrow}$, we can produce a bichromatic Hamiltonian:

$$H_{\text{bic}} = \hbar\eta\frac{\Omega_{\uparrow\downarrow}}{2}(\sigma_x\cos\phi_+ - \sigma_y\sin\phi_+) \otimes [(a^\dagger + a)\cos\phi_- + i(a^\dagger - a)\sin\phi_-], \quad (5)$$

in which we denote ϕ_b and ϕ_r as the phases of the light fields that are blue and red detuned by ω, respectively, and set $\phi_+ = \frac{\phi_\text{b}+\phi_\text{r}}{2} + \frac{\pi}{2}$, $\phi_- = \frac{\phi_\text{b}-\phi_\text{r}}{2}$ as the sum and difference of the phases of these light fields.

By setting different phases ϕ_+ and ϕ_-, we can drive the displacement in the x or y direction, respectively. In this work, when a controlled displacement in the x direction needs to be driven, we set the phase to be $\phi_+^x = \phi_-^x = 0$, and set the duration time of this bichromatic pulse to be $t = 2|\alpha|/(\eta\Omega_{\uparrow\downarrow})$. Under this setting, one can find that Eq. (5) reduces to $H_{\text{bic}}^x = \hbar\eta\frac{\Omega_{\downarrow\uparrow}}{2}\sigma_x\otimes(a^\dagger + a)$. For the initial state $|\psi_0\rangle = |\pm\rangle|0\rangle$, where $|\pm\rangle = \frac{1}{\sqrt{2}}(|\uparrow\rangle \pm |\downarrow\rangle)$, a displaced coherent state can be created by this bichromatic pulse: $|\psi\rangle = e^{-iH_{\text{bic}}^x t/\hbar}|+\rangle|0\rangle = |+\rangle D(-i\eta\Omega_{\uparrow\downarrow}t/2)|0\rangle = |+\rangle|-i|\alpha|\rangle$, or $|\psi\rangle = e^{-iH_{\text{bic}}^x t/\hbar}|-\rangle|0\rangle = |-\rangle D(+i\eta\Omega_{\uparrow\downarrow}t/2)|0\rangle = |-\rangle|+i|\alpha|\rangle$.[45] Therefore, the displacement in the x direction can be decided by the walker's internal states under the basis of $\{|+\rangle, |-\rangle\}$, and the shift operator S_x can be constructed as $S_x = R_x e^{-iH_{\text{bic}}^x t/\hbar}R_x$, where $R_x = \frac{1}{\sqrt{2}}\left(\begin{smallmatrix}1 & 1\\ 1 & -1\end{smallmatrix}\right)$ converts $\{|\uparrow\rangle, |\downarrow\rangle\}$ to $\{|+_x\rangle, |-_x\rangle\}$. Similarly, when a controlled displacement in the y direction needs to be driven, we set the phase to be $\phi_+^y = \phi_-^y = \pi/2$, so that Eq. (5) reduces to $H_{\text{bic}}^y = -\hbar\eta\frac{\Omega_{\downarrow\uparrow}}{2}\sigma_y\otimes i(a^\dagger - a)$. The shift operator S_y can be constructed as $S_y = R_y e^{-iH_{bic}^y t/\hbar}R_y$, where $R_y = \frac{1}{\sqrt{2}}\left(\begin{smallmatrix}1 & 1\\ i & -i\end{smallmatrix}\right)$ converts $\{|\uparrow\rangle, |\downarrow\rangle\}$ to $\{|+_y\rangle, |-_y\rangle\}$.

Quantum Walk on a 2D Phase Lattice of an Ion. As mentioned above, we need to first verify the feasibility of this scheme under experimental parameters. For a single bounded $^{40}Ca^+$ ion in a linear Paul trap, the motional trap frequency ω is usually around $\omega = 2\pi\times 2\,\text{MHz}$, the Lamb–Dicke parameter η of $^{40}Ca^+$ ion driven by 729 nm laser is set to 0.07 as an example. We set the distance of a single walking step in the x or y directions to be $|\alpha_x| = |\alpha_y| = 2$, so that the displaced states are highly separable. The duration time of the bichromatic pulse can be calculated as $t_x = t_y = 2|\alpha_{x,\,y}|/(\eta\Omega_{\downarrow\uparrow}) = 45.47\,\mu\text{s}$, which is also consistent with the usual duration time of laser pulses in ion trap experiments.[46]

In this work, the walker with an initial internal state $\frac{1}{\sqrt{2}}(|\uparrow\rangle + i|\downarrow\rangle)$ starts from the lattice's origin position of $(0, 0)$, which corresponds to the initial oscillator state $|0\rangle$, as shown in Fig. 2(a). For each discrete time step, the walker state is periodically driven by the Floquet operator $U = M_y S_y C M_x S_x C$ using the laser-ion interaction model we have constructed before. Here we take Figs. 2(a) and 2(b) as an example to explain the discrete walking results after one step of the Floquet operator U. Since the probability distributions of the initial internal state on the $\{|+_{x,\,y}\rangle, |-_{x,\,y}\rangle\}$ states are the same after rotations, the overall probability of displacements $D(\pm\alpha_{x,\,y})$ should also be the same. Thus, the controlled displacements in the x and y directions will eventually produce a 2D cat state, as shown in Fig. 2(b).

Within three walking steps, we analyze the directional displacement of the walker state by calculating the Wigner function of the oscillator state. In the absence of gain-loss operators $\gamma_x = \gamma_y = 0$, quantum walks driven by U show a symmetric propagation along the 2D lattice. In Fig. 2, we show the calculated quasiprobability distribution of the

lattice sites from step = 0 to step = 3, verifying that the coin degree of freedom is transferred during the dynamics of the DTQW.

NHSE and Tunable Bulk Flow. We then focus on the NHSE on the dynamics of DTQWs. Under the finite gain-loss parameters $\gamma_{x,\,y}$ along the x and y directions, the final quasiprobability distribution becomes asymmetric with a preferred direction. For example, when $|\gamma_x| = |\gamma_y| \neq 0$, half the displacements are suppressed for both the x and y directions. Thus, the bulk flow should be diagonal to the square lattice. By tuning the ratio of γ_y/γ_x, we can adjust the direction of the asymmetric quasiprobability distribution in the lattice. In Fig. 3, we show the calculated quasiprobability distribution of the lattice sites after three walking steps under different ratios of γ_y/γ_x. As shown in Figs. 3(a)–3(d), we adjust the positive-negative dissipation values along the x and y directions separately and keep $|\gamma_y/\gamma_x| = 1$. Correspondingly, a diagonal polar angle of the bulk flow is observed to vary between $\{-3\pi/4,\, \pi/4,\, -\pi/4,\, 3\pi/4\}$ in the square lattice.

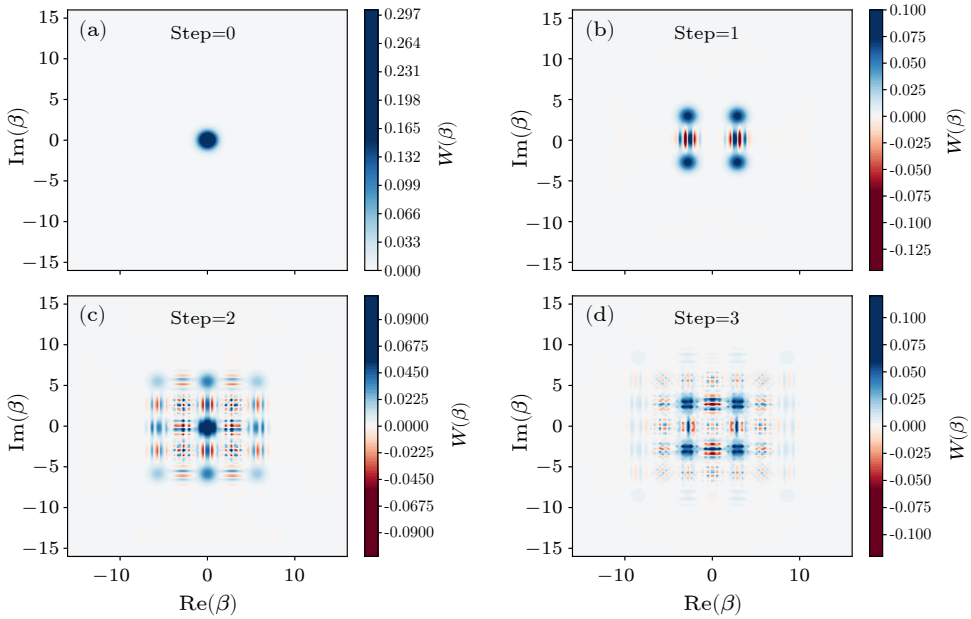

Fig. 2. Wigner functions $W(\beta)$ for a Hermitian 2D quantum walk with $\gamma_x = \gamma_y = 0$ from step = 0 to step = 3. The horizontal and vertical axes show the real and imaginary components of β, respectively. The color bar indicates the calculated value of the Wigner function. Other parameters are $|\alpha_x| = |\alpha_y| = 2$, $\omega = 2\pi \times 2\,\text{MHz}$, $\Omega_{\downarrow\uparrow} = 2\pi \times 0.2\,\text{MHz}$, and $\eta = 0.07$, as defined in the text. We observe coherent quantum walks along the discretized lattice consisting of displaced coherent states. Along with the propagation in the lattice, we also observe a highly non-uniform distribution of the lattice population, which we attribute to coherent interference.

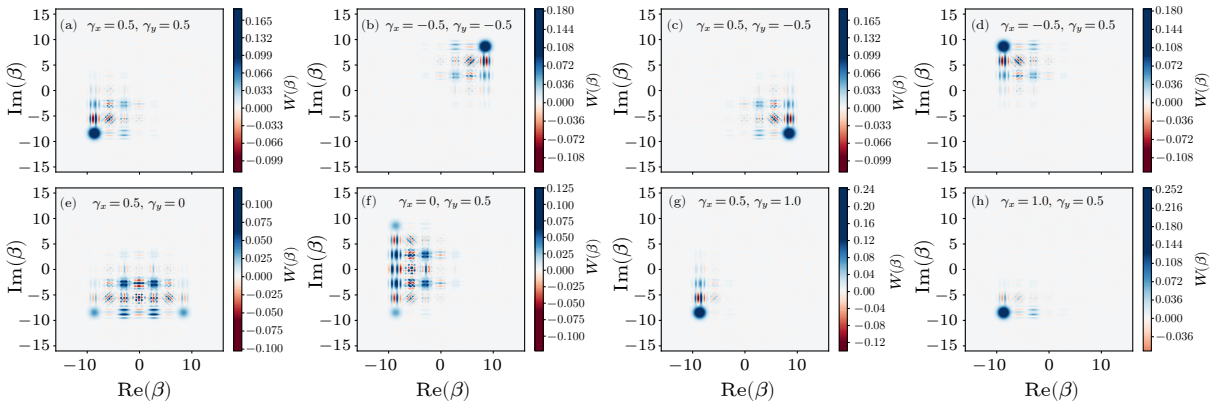

Fig. 3. Wigner functions $W(\beta)$ for a non-Hermitian quantum walk with step = 3 and various γ_y/γ_x values. The color bar indicates the calculated value of the Wigner function. Other parameters are $|\alpha_x| = |\alpha_y| = 2$, $\omega = 2\pi \times 2\,\text{MHz}$, $\Omega_{\downarrow\uparrow} = 2\pi \times 0.2\,\text{MHz}$, and $\eta = 0.07$, as defined in the text. In (a)–(d), the positive-negative dissipation values of the ratio γ_y/γ_x are adjusted between ± 1 while $|\gamma_y/\gamma_x| = 1$. (e) The bulk flow is suppressed only in the x direction when $|\gamma_y/\gamma_x| = 0$. (f) The bulk flow is suppressed only in the y direction when $|\gamma_x/\gamma_y| = 0$. (g) Asymmetric quasiprobability distribution along the diagonal line with $|\gamma_y/\gamma_x| = 2$. (h) Asymmetric quasiprobability distribution along the diagonal line with $|\gamma_x/\gamma_y| = 2$.

When $|\gamma_y/\gamma_x|$ varies, the direction of displacement after quantum walks can be continuously tuned. For example, in Figs. 3(e) and 3(f) we adjust $|\gamma_y/\gamma_x|$ in $\{0,\ \infty\}$ for three-step quantum walks. It can be observed that when the gain-loss parameter is 0 in one direction and has a finite value in the other direction, the bulk flow in the latter direction will be suppressed so that the final quasiprobability is only distributed in half of the lattice. When $|\gamma_y/\gamma_x| = 2$, as shown in Fig. 3(g), the lattice site with the highest quasiprobability is still the diagonal lattice point at an angle of $-3\pi/4$ with the position of $(-3\alpha_x, -3\alpha_y)$. However, when compared with Fig. 3(a), it is also obvious that the quasiprobability distribution of the lattice is no longer symmetrical with the diagonal line, and it will be more preferred towards the direction with a smaller loss parameter. These observed loss-induced directional bulk flows directly show the orientation of directional matter transport under open boundary conditions, which is closely related to the NHSE in 2D.

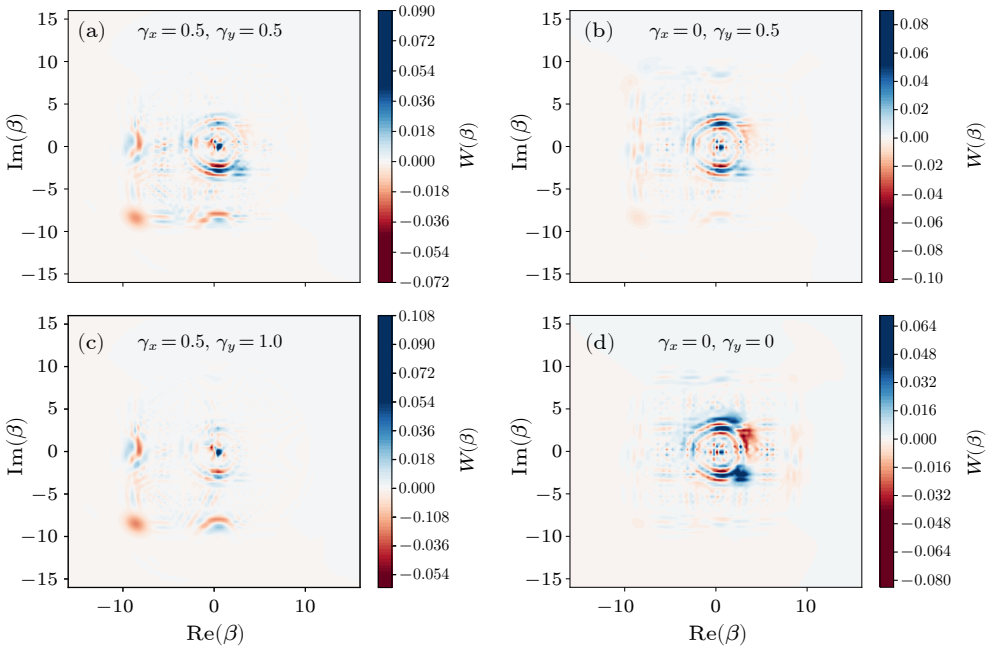

Fig. 4. Wigner functions $W(\beta)$ for a non-Hermitian quantum walk with step = 3 and various $\gamma_{x,\,y}$ values under the Lindblad master equation. The color bar indicates the calculated value of the Wigner function. Other parameters are $|\alpha_x| = |\alpha_y| = 2$, $\omega = 2\pi \times 2\,\text{MHz}$, $\Omega_{\downarrow\uparrow} = 2\pi \times 0.2\,\text{MHz}$, $\eta = 0.07$, $\dot{\bar{n}} = 0.2\,\text{quanta/s}$, $T_2^{\text{m}} = 35\,\text{ms}$, and $T_2^{\text{s}} = 40\,\text{ms}$, defined in the text. We observe similar bulk flows as those we simulated before in Figs. 2 and 3. (a) The bulk flow is diagonal to the square lattice with $\gamma_x = \gamma_y = 0.5$, corresponding to Fig. 3(a). (b) The bulk flow is suppressed only in the y direction with $|\gamma_x/\gamma_y| = 0$, corresponding to Fig. 3(f). (c) Asymmetric quasiprobability distribution along the diagonal line with $|\gamma_y/\gamma_x| = 2$, corresponding to Fig. 3(g). (d) Symmetric propagation along the 2D square lattice with $\gamma_x = \gamma_y = 0$, corresponding to Fig. 2(d).

Effects with Experimental Imperfections. For the above numerical simulation, we have neglected the decoherence of the oscillator mode from motional heating and dephasing, and the decoherence of the spin state, which are the dominant noises in the ion trap systems. To account for the impact of these noises in the experimental systems, we consider the full Lindblad master equation:

$$\frac{d\rho}{dt} = \frac{1}{i\hbar}[H,\,\rho] + \sum_j \left(L_j \rho L_j^\dagger - \frac{1}{2} L_j^\dagger L_j \rho - \frac{1}{2}\rho L_j^\dagger L_j\right), \quad (6)$$

in which the dissipation operators are $L_{\text{heat}} = \sqrt{\dot{\bar{n}}}a^\dagger$, $L_{\text{cool}} = \sqrt{\dot{\bar{n}}}a$, $L_{\text{motion}} = \sqrt{1/T_2^{\text{m}}}a^\dagger a$, and $L_{\text{spin}} = \sqrt{1/T_2^{\text{s}}}\sigma_z$. Here $\dot{\bar{n}}$ represents the heating rate of the oscillator, T_2^{m} represents the motional dephasing time, and T_2^{s} represents the spin qubit dephasing time. We now take the above imperfections into account for numerical calculations with some typical values of $\dot{\bar{n}} = 0.2\,\text{quanta/s}$, $T_2^{\text{m}} = 35\,\text{ms}$,[47] and $T_2^{\text{s}} = 40\,\text{ms}$.[48]

Including these possible decoherence sources, in Fig. 4 we show numerical simulation results on the NHSE of DTQWs under the full Lindblad master equation, with various $\gamma_{x,\,y}$ values at step = 3. In Fig. 4(a), we set $\gamma_x = \gamma_y = 0.5$, which is consistent with Fig. 3(a), so that the bulk flow should be diagonal to the square lattice. It can be observed that with the imperfections in the experiment, the coherence between walker states and the fidelity of preparation are both suppressed, but a bulk flow with a diagonal polar angle of $-3\pi/4$ is still observable. In Figs. 4(b) and 4(c), we consider the case of $|\gamma_y/\gamma_x| \neq 1$, so that the final quasiprobability distribution should become asymmetric with a preferred direction. In Fig. 4(b) we observe suppression of the bulk flow in the y direction with $|\gamma_x/\gamma_y| = 0$ and the result is similar to Fig. 3(f). In Fig. 4(c), we set the loss parameter to be greater in the y direction than x direction with $|\gamma_y/\gamma_x| = 2$. It can be observed that the quasiprobability distribution of the lattice is changed from a diagonal distribution along the angle

of $-3\pi/4$, while in Fig. 4(a) it is more preferred towards the x direction with a smaller loss parameter. Figure 4(c) provides a very similar result compared to Fig. 3(g) in the sense of directional bulk flow, in addition to slight components at the center and along the imaginary axis, which we attribute to alternation of the dynamics due to decoherence. Finally, in Fig. 4(d), we simulate the result in the absence of gain-loss operators with $\gamma_x = \gamma_y = 0$ as a sanity check, and observed an imperfect symmetric propagation along the 2D lattice when compared with Fig. 2(d), in which the asymmetry along the x and y directions is due to uneven dissipation caused by the sequential x- and y-displacement operations. These numerical simulation results confirm that even with experimental imperfections, the dynamic signatures of the NHSE can still be observed and manipulated through gain-loss parameters, showing the feasibility of our 2D DTQW scheme.

In conclusions, we have proposed an experimental scheme to realize 2D quantum walks in the momentum phase space of a single trapped ion. With numerical simulations, we demonstrate loss-induced directional bulk flows with adjustable orientations, which is one of the major features of NHSE. Since the theoretical models here can all be achieved in an ion trap platform through single-qubit rotation operations and laser pulses, this highly practical scheme can be exploited for higher-dimensional quantum walk device design, as well as the investigation of complex quantum systems, including non-Hermitian physics in open systems and directional dynamics in topological transport.

Acknowledgements. We thank W. Yi for helpful discussion. This work was supported by the National Natural Science Foundation of China (Grant Nos. 92165206 and 11974330), the Innovation Program for Quantum Science and Technology (Grant No. 2021ZD0301603), and the Fundamental Research Funds for the Central Universities.

References

[1] Aharonov Y, Davidovich L, and Zagury N 1993 *Phys. Rev. A* **48** 1687
[2] Kempe J 2003 *Contemp. Phys.* **44** 307
[3] Kadian K, Garhwal S, and Kumar A 2021 *Comput. Sci. Rev.* **41** 100419
[4] Childs A M and Goldstone J 2004 *Phys. Rev. A* **70** 042312
[5] Portugal R 2016 *Phys. Rev. A* **93** 062335
[6] Potoček V, Gábris A, Kiss T, and Jex I 2009 *Phys. Rev. A* **79** 012325
[7] Chakraborty S, Novo L, Ambainis A, and Omar Y 2016 *Phys. Rev. Lett.* **116** 100501
[8] Campbell E, Khurana A, and Montanaro A 2019 *Quantum* **3** 167
[9] Farhi E, Goldstone J, and Gutmann S 2008 *Theory Comput.* **4** 169
[10] Douglas B L and Wang J B 2008 *J. Phys. A* **41** 075303
[11] Bruderer M and Plenio M B 2016 *Phys. Rev. A* **94** 062317
[12] Kitagawa T, Rudner M S, Berg E, and Demler E 2010 *Phys. Rev. A* **82** 033429
[13] Zhang W W, Goyal S K, Gao F, Sanders B C, and Simon C 2016 *New J. Phys.* **18** 093025
[14] Xiao L, Zhan X, Bian Z H *et al.* 2017 *Nat. Phys.* **13** 1117
[15] Bepari K, Malik S, Spannowsky M, and Williams S 2022 *Phys. Rev. D* **106** 056002
[16] Rohde P P, Fitzsimons J F, and Gilchrist A 2012 *Phys. Rev. Lett.* **109** 150501
[17] Chandrashekar C M and Busch T 2014 *Sci. Rep.* **4** 6583
[18] Wang Y, Shang Y, and Xue P 2017 *Quantum Inf. Process.* **16** 221
[19] Xue P, Zhang R, Qin H, Zhan X, Bian Z H, Li J, and Sanders B C 2015 *Phys. Rev. Lett.* **114** 140502
[20] Zhan X, Xiao L, Bian Z H, Wang K K, Qiu X Z, Sanders B C, Yi W, and Xue P 2017 *Phys. Rev. Lett.* **119** 130501
[21] Flurin E, Ramasesh V V, Hacohen-Gourgy S, Martin L S, Yao N Y, and Siddiqi I 2017 *Phys. Rev. X* **7** 031023
[22] Leibfried D, Blatt R, Monroe C, and Wineland D 2003 *Rev. Mod. Phys.* **75** 281
[23] Schmitz H, Matjeschk R, Schneider C, Glueckert J, Enderlein M, Huber T, and Schaetz T 2009 *Phys. Rev. Lett.* **103** 090504
[24] Zähringer F, Kirchmair G, Gerritsma R, Solano E, Blatt R, and Roos C F 2010 *Phys. Rev. Lett.* **104** 100503
[25] Meng Y, Mei F, Chen G, and Jia S T 2020 *Chin. Phys. B* **29** 070501
[26] Zhang H Q, Ai M Z, Cui J M, Han Y J, Li C F, and Guo G C 2021 *Phys. Rev. A* **104** 022213
[27] Lin Q, Qin H, Wang K K, Xiao L, and Xue P 2020 *Chin. Phys. B* **29** 110303
[28] Okuma N, Kawabata K, Shiozaki K, and Sato M 2020 *Phys. Rev. Lett.* **124** 086801
[29] Li T Y, Sun J Z, Zhang Y S, and Yi W 2021 *Phys. Rev. Res.* **3** 023022
[30] Zou D Y, Chen T, He W J, Bao J C, Lee C H, Sun H J, and Zhang X D 2021 *Nat. Commun.* **12** 7201
[31] Li Y H, Liang C, Wang C Y, Lu C C, and Liu Y C 2022 *Phys. Rev. Lett.* **128** 223903
[32] Yao Y Y, Xiang L, Guo Z X *et al.* 2023 *Nat. Phys.* **19** 1459
[33] Lin C Y, Su W C, and Wu S T 2020 *Quantum Inf. Process.* **19** 272
[34] Lin Q, Yi W, and Xue P 2023 *Nat. Commun.* **14** 6283
[35] Lin Z G, Lin Y H, and Yi W 2022 *Phys. Rev. A* **106** 063112
[36] Longhi S 2019 *Phys. Rev. Res.* **1** 023013
[37] Liang Q, Xie D Z, Dong Z L, Li H W, Li H, Gadway B, Yi W, and Yan B 2022 *Phys. Rev. Lett.* **129** 070401
[38] Lin Q, Li T Y, Xiao L, Wang K K, Yi W, and Xue P 2022 *Phys. Rev. Lett.* **129** 113601
[39] Leibfried D, Meekhof D M, King B E, Monroe C, Itano W M, and Wineland D J 1996 *Phys. Rev. Lett.* **77** 4281
[40] Kienzler D, Flühmann C, Negnevitsky V, Lo H Y, Marinelli M, Nadlinger D, and Home J P 2016 *Phys. Rev. Lett.* **116** 140402
[41] Ding S Q, Maslennikov G, Hablützel R, Loh H Q, and Matsukevich D 2017 *Phys. Rev. Lett.* **119** 150404
[42] Flühmann C and Home J P 2020 *Phys. Rev. Lett.* **125** 043602
[43] Clark C R, Tinkey H N, Sawyer B C *et al.* 2021 *Phys. Rev. Lett.* **127** 130505
[44] Lee P J, Brickman K A, Deslauriers L, Haljan P C, Duan L M, and Monroe C 2005 *J. Opt. B* **7** S371
[45] Monroe C, Meekhof D M, King B E, and Wineland D J 1996 *Science* **272** 1131
[46] Hempel C, Lanyon B P, Jurcevic P *et al.* 2013 *Nat. Photon.* **7** 630
[47] Valahu C H, Olaya-Agudelo V C, MacDonell R J *et al.* 2023 *Nat. Chem.* **15** 1503
[48] Hempel C, Maier C, Romero J *et al.* 2018 *Phys. Rev. X* **8** 031022